LUND UNIVERSITY

On the design of optimal measurements for antenna near-field imaging problems

Nordebo, Sven; Gustafsson, Mats

2006

Link to publication

Citation for published version (APA):
Nordebo, S., & Gustafsson, M. (2006). *On the design of optimal measurements for antenna near-field imaging problems.* (Technical Report LUTEDX/(TEAT-7142)/1-17/(2006); Vol. TEAT-7142). [Publisher information missing].

Total number of authors:
2

General rights
Unless other specific re-use rights are stated the following general rights apply:
Copyright and moral rights for the publications made accessible in the public portal are retained by the authors and/or other copyright owners and it is a condition of accessing publications that users recognise and abide by the legal requirements associated with these rights.
• Users may download and print one copy of any publication from the public portal for the purpose of private study or research.
• You may not further distribute the material or use it for any profit-making activity or commercial gain
• You may freely distribute the URL identifying the publication in the public portal

Read more about Creative commons licenses: https://creativecommons.org/licenses/

Take down policy
If you believe that this document breaches copyright please contact us providing details, and we will remove access to the work immediately and investigate your claim.

LUND UNIVERSITY

PO Box 117
221 00 Lund
+46 46-222 00 00

Download date: 23. Dec. 2025

CODEN:LUTEDX/(TEAT-7142)/1-17/(2006)

On the Design of Optimal Measurements for Antenna Near-Field Imaging Problems

Sven Nordebo and Mats Gustafsson

Department of Electroscience
Electromagnetic Theory
Lund Institute of Technology
Sweden

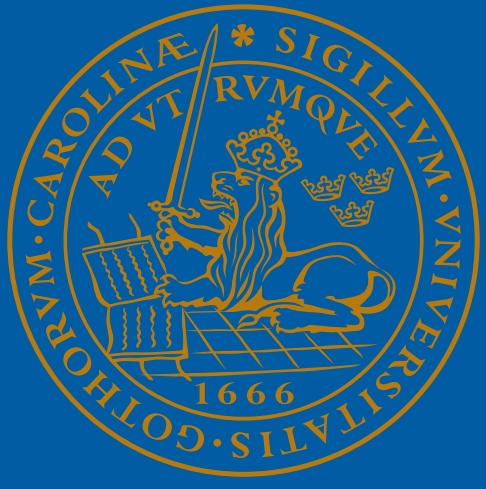

Sven Nordebo
Sven.Nordebo@msi.vxu.se

School of Mathematics and Systems Engineering
Växjö University
351 95 Växjö
Sweden

Mats Gustafsson
Mats.Gustafsson@es.lth.se

Department of Electroscience
Electromagnetic Theory
Lund Institute of Technology
P.O. Box 118
SE-221 00 Lund
Sweden

Editor: Gerhard Kristensson
© Sven Nordebo and Mats Gustafsson, Lund, February 2, 2006

Abstract

A mathematical framework is introduced for optimization of antenna near-field imaging problems, based on the multipole expansion of the electromagnetic field, the *Fisher information* to quantify the quality of data and use of modern interior point convex optimization techniques. We consider the general problem of optimizing the measurement sensor allocation for parameter estimation in distributed systems, and in particular the problem of optimizing the measurement set-up for antenna near-field estimation. As an application example for antenna near-field imaging, we consider a relevant measurement set-up using cylindrical probing coordinates. The convex optimization problem is examined using duality theory, and it is shown that several structural properties of the optimal measurement problem can be exploited in developing an efficient interior point optimization method. In particular, we show that the cylindrical measurement set-up yields a Fisher information matrix with block diagonal structure, a feature which can be directly exploited in the optimization algorithm by reducing the number of dual decision variables.

1 Introduction

Inverse scattering and imaging are topics with a variety of applications in *e.g.*, medicine, non-destructive testing, surveillance, quantum mechanics, optics, etc. These problems are in general ill-posed, *i.e.*, they are not well-posed in the sense of existence, uniqueness, and continuous dependence of the solution on the data [4, 5, 8, 11–14]. Although imaging and inverse scattering have been thoroughly studied during the last century there is only a partial understanding of these complex problems. Most of the efforts have been placed on the development of efficient inversion algorithms and mathematical uniqueness results. In comparison, there are very few results and a limited knowledge about the information content in the inversion data and the design of optimal measurement geometries.

Optimal experimental design constitutes a broad area that has been evolving since the 80's, see *e.g.*, [2, 19, 23, 25]. Typical application areas of experimental design are for optimization of various industrial production processes, see *e.g.*, [3]. However, there seem to be very few applications to imaging and inverse scattering and only a few studies have been devoted to the sensor location problem for parameter estimation. Qureshi et. al. [20] developed an optimality criterion based on the determinant of the Fisher information matrix, a topic which has been further developed in *e.g.*, [22, 25]. The convex Fisher information measure was proposed already in the early 80's [20], but a comprehensive exploitation of the efficient polynomial time interior point methods for convex optimization that has been established during the 90's (including determinant maximization) seem to be missing, see *e.g.*, [7, 15, 24].

Previously, we have employed linear estimation theory and the Cramér-Rao lower bound to quantify the ill-posedness of inverse problems, see *e.g.*, [16, 18]. The purpose of this paper is to provide a mathematical framework for optimization of inverse imaging problems, based on the multipole expansion of the electromagnetic

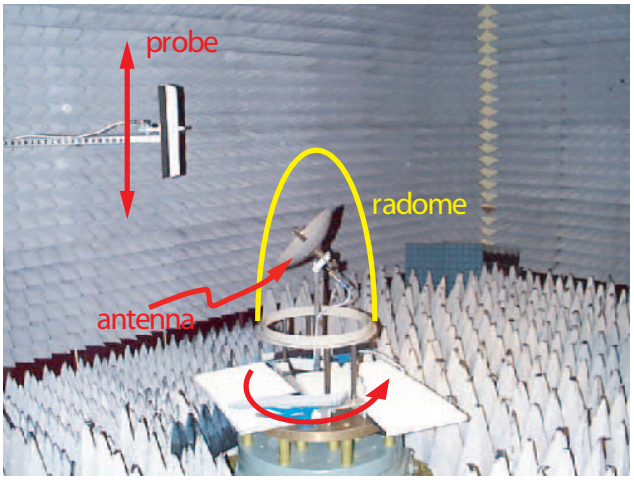

Figure 1: Measurement setup for antenna near field imaging using cylindrical probing coordinates.

field [1, 6, 9], the *Fisher information* [10] to quantify the quality of data and use of modern interior point convex optimization techniques [7, 15, 24].

As a prototype example of designing optimal measurements for antenna near-field imaging, we study the measurement set-up[1] depicted in Figure 1. The cylindrical data is gathered by rotating the object under test and moving the near-field probe in the vertical direction. The measurements are time consuming and hence costly. The azimuthal measurement points are determined by the angular velocity of the object under test and are in general fixed. The measurement can hence only be improved by proper choice of the vertical measurement points. By Fourier transforming the data over the azimuthal coordinates the Fisher information matrix decouples and obtains a block diagonal structure. From convex optimization theory we know that the dual of the *log*-determinant problem [15] encompasses as many dual variables as there are nonzero elements of the Fisher information matrix. Hence, a decoupled Fisher information matrix will impose a very specific structure also on the convex optimization problem. This is a vital point to take advantage of in developing a numerically efficient optimization method for an inverse imaging problem that may in general be very large.

2 Antenna near-field estimation based on cylindrical data

We consider the antenna near-field estimation problem based on cylindrical data. Let (r, θ, ϕ) and (ρ, ϕ, z) denote the spherical and cylindrical coordinates, respectively. Further, let $k = \omega/c$ denote the wave number, $\omega = 2\pi f$ the angular frequency, and

[1]The picture is taken at an antenna near-field measurement campaign performed by SAAB Bofors Dynamics and Chelton Applied Composites, Sweden.

c and η the speed of light and the wave impedance of free space, respectively.

Assume that all sources are contained inside a sphere of radius $r = a$, and let $e^{\mathrm{i}\omega t}$ be the time-convention. The transmitted electric field, $\boldsymbol{E}(\boldsymbol{r})$, can then be expanded in *outgoing spherical vector waves* $\boldsymbol{u}_{\tau ml}(k\boldsymbol{r})$ for $r > a$ as [1, 6, 9]

$$\boldsymbol{E}(\boldsymbol{r}) \;=\; \sum_{l=1}^{\infty}\sum_{m=-l}^{l}\sum_{\tau=1}^{2} f_{\tau ml}\boldsymbol{u}_{\tau ml}(k\boldsymbol{r}) \tag{2.1}$$

where $f_{\tau ml}$ are the multipole coefficients. Here $\tau = 1$ corresponds to a transversal electric (TE) wave and $\tau = 2$ corresponds to a transversal magnetic (TM) wave. The other indices are $l = 1, 2, \ldots, \infty$ and $m = -l \ldots, l$ where l denotes the *order* of that mode. In principle, the sum in (2.1) is infinite. However, for all practical purposes the maximum useful order L is finite and is physically restricted by the electrical size ka of the sphere as well as the bandwidth of the antenna, see *e.g.*, [6, 17]. For further details about the spherical vector mode representation we refer to the Appendix and [1, 6, 9].

We consider now the inverse, linear estimation problem of determining the multipole coefficients $f_{\tau ml}$ based on an observation of the electric near field, $\boldsymbol{E}(\boldsymbol{r})$, as it is measured on the cylindrical surface $\{\rho = \rho_0, z_1 \leq z \leq z_2\}$. We assume that the measurement is corrupted by additive and spatially uncorrelated complex Gaussian noise $\boldsymbol{N}(\boldsymbol{r})$ with zero mean and dyadic covariance function $\mathcal{E}\{\boldsymbol{N}(\boldsymbol{r})\boldsymbol{N}^*(\boldsymbol{r}')\} = \sigma_{\mathrm{n}}^2\delta(\boldsymbol{r}-\boldsymbol{r}')\mathbf{I}$ where $\mathcal{E}\{\cdot\}$ denotes the expectation operator, σ_{n}^2 the noise variance, $\delta(\boldsymbol{r})$ the impulse function and $\mathbf{I}$ the identity dyad. Note that since the data is assumed here to be discrete, $\delta(\cdot)$ denotes the discrete impulse function with $\delta(0) = 1$.

When we wish to estimate the near field at a sphere of radius $r = a$, the linear equations in (2.1) are first regularized by normalizing with the vector norm $\|\boldsymbol{u}_{\tau ml}(k\boldsymbol{r})\| = (\int |\boldsymbol{u}_{\tau ml}(k\boldsymbol{r})|^2 \,\mathrm{d}\Omega)^{1/2}$ where $\mathrm{d}\Omega$ is the differential solid angle. By the orthonormality of the spherical vector harmonics [1, 6, 9], we have

$$\begin{aligned}
\|\boldsymbol{u}_{1ml}(k\boldsymbol{r})\|_{r=a}^2 &= \left|\mathrm{h}_l^{(2)}(ka)\right|^2 \\
\|\boldsymbol{u}_{2ml}(k\boldsymbol{r})\|_{r=a}^2 &= \left|\frac{(ka\mathrm{h}_l^{(2)}(ka))'}{ka}\right|^2 + l(l+1)\left|\frac{\mathrm{h}_l^{(2)}(ka)}{ka}\right|^2
\end{aligned} \tag{2.2}$$

which are independent of the azimuthal m-index.

Consider first a situation where we have arbitrary measurement points $\boldsymbol{r}_j$ for $j = 1, \ldots, n$. The Fisher information matrix [10] for estimating the normalized multipole coefficients $f_{\tau ml}$ is then given by

$$\begin{aligned}
[\boldsymbol{\mathcal{I}}]_{\tau ml,\tau' m' l'} &= \frac{1}{\sigma_{\mathrm{n}}^2}\sum_{j=1}^{n}\frac{\partial \boldsymbol{E}^*(\boldsymbol{r}_j)}{\partial f_{\tau ml}^*}\cdot\frac{\partial \boldsymbol{E}(\boldsymbol{r}_j)}{\partial f_{\tau' m' l'}} \\
&= \frac{1}{\sigma_{\mathrm{n}}^2}\sum_{j=1}^{n}\frac{\boldsymbol{u}_{\tau ml}^*(k\boldsymbol{r}_j)}{\|\boldsymbol{u}_{\tau ml}(k\boldsymbol{r})\|_{r=a}}\cdot\frac{\boldsymbol{u}_{\tau' m' l'}(k\boldsymbol{r}_j)}{\|\boldsymbol{u}_{\tau' m' l'}(k\boldsymbol{r})\|_{r=a}}.
\end{aligned} \tag{2.3}$$

Now, assume that we have a cylindrical measurement using M azimuthal points ϕ equally spaced in $[0, 2\pi]$, and n vertical positions z_j with spherical coordinates (r_j, θ_j). The Fisher information (2.3) then becomes

$$[\boldsymbol{\mathcal{I}}]_{\tau ml,\tau' m' l'} = \frac{M}{\sigma_{\mathrm{n}}^2} \sum_{j=1}^{n} \frac{\tilde{\boldsymbol{u}}^*_{\tau ml}(r_j,\theta_j)}{\|\boldsymbol{u}_{\tau ml}(k\boldsymbol{r})\|_{r=a}} \cdot \frac{\tilde{\boldsymbol{u}}_{\tau' m' l'}(r_j,\theta_j)}{\|\boldsymbol{u}_{\tau' m' l'}(k\boldsymbol{r})\|_{r=a}} \delta(m-m') \tag{2.4}$$

where we have employed the orthogonality of the Discrete Fourier Transform (DFT) and the azimuthal Fourier transform $\tilde{\boldsymbol{u}}_{\tau ml}(r,\theta)$ of the spherical vector waves $\boldsymbol{u}_{\tau ml}(k\boldsymbol{r}) = \tilde{\boldsymbol{u}}_{\tau ml}(r,\theta)\mathrm{e}^{\mathrm{i}m\phi}$, see the Appendix.

The Fisher information matrix (2.4) is decoupled over the m-index and can hence be organized as a block diagonal matrix with diagonal blocks $\boldsymbol{\mathcal{I}}_m$ with $[\boldsymbol{\mathcal{I}}_m]_{\tau l,\tau' l'} = [\boldsymbol{\mathcal{I}}]_{\tau ml,\tau' ml'}$ for $-L \leq m \leq L$ where $\tau, \tau' = 1, 2$ and $l, l' = \max\{|m|, 1\}, \ldots, L$. The corresponding Cramér-Rao lower bound (CRB) [10] for near-field estimation is now given by

$$\mathcal{E}\left\{|\boldsymbol{E}^{\mathrm{e}}(\boldsymbol{r}) - \boldsymbol{E}(\boldsymbol{r})|^2\right\} \geq \sum_{m=-L}^{L} \sum_{\tau,\tau'=1}^{2} \sum_{l,l'=\max\{|m|,1\}}^{L} \frac{\tilde{\boldsymbol{u}}^*_{\tau ml}(r,\theta) \cdot [\boldsymbol{\mathcal{I}}_m^{-1}]_{\tau l,\tau' l'} \tilde{\boldsymbol{u}}_{\tau' ml'}(r,\theta)}{\|\boldsymbol{u}_{\tau ml}(k\boldsymbol{r})\|_{r=a} \|\boldsymbol{u}_{\tau' ml'}(k\boldsymbol{r})\|_{r=a}} \tag{2.5}$$

where $\boldsymbol{E}^{\mathrm{e}}(\boldsymbol{r})$ denotes the estimated field. Note that the CRB in (2.5) is independent of the azimuthal coordinate ϕ, and depends only on (r, θ).

3 The convex problem of optimal measurements

The problem of designing optimal measurements is to determine a set of optimal observation points $\boldsymbol{r}_j$ which maximizes a suitable chosen measure of the estimation performance. We will follow here the approach proposed in *e.g.*, [20, 22, 25] by defining a constrained convex functional of the Fisher information matrix.

Assume that there are n possible spatial observation points $\boldsymbol{r}_j$ and assign to each point the probability measure $x_j \geq 0$ for $j = 1, \ldots, n$. The corresponding vector decision variable is denoted $\mathbf{x} \in \mathbb{R}^n$. Let $\mathbf{G}(\mathbf{x})$ denote the *Fisher information matrix* corresponding to a specific measurement constellation $\mathbf{x}$, $\boldsymbol{\xi} \in \mathbb{C}^\nu$ the vector of complex parameters to be estimated, ν the number of parameters and $\frac{\partial \boldsymbol{E}(\boldsymbol{r}_j)}{\partial \boldsymbol{\xi}}$ the corresponding sensitivity vector, see *e.g.*, the previous model (2.3). It is further assumed that the observations are degraded by additive uncorrelated complex Gaussian noise with variance σ_{n}^2. The corresponding convex optimization problem is then given by

$$\begin{cases} \min\limits_{\mathbf{x}\in\mathbb{R}^n} -\log\det \mathbf{G}(\mathbf{x}) \\ \mathbf{G}(\mathbf{x}) = \frac{1}{\sigma_{\mathrm{n}}^2} \sum\limits_{j=1}^{n} x_j \dfrac{\partial \boldsymbol{E}^*(\boldsymbol{r}_j)}{\partial \boldsymbol{\xi}^*} \cdot \dfrac{\partial \boldsymbol{E}(\boldsymbol{r}_j)}{\partial \boldsymbol{\xi}^{\mathrm{T}}} \\ \mathbf{x} \geq \mathbf{0} \\ \sum\limits_{j=1}^{n} x_j \leq 1 \end{cases} \tag{3.1}$$

which is equivalent to maximize the determinant of the Fisher information matrix.

In order to gain insight about the optimization problem in (3.1) and to solve it efficiently we now derive the corresponding dual formulation. See e.g. [24] for a similar derivation with linear semidefinite constraints. The optimization problem (3.1) is first rewritten on the canonical primal form (P)

$$(\mathrm{P}) \begin{cases} \min\limits_{\mathbf{x}\in\mathbb{R}^n} -\log\det \mathbf{G}(\mathbf{x}) \\ \mathbf{G}(\mathbf{x}) = \sum\limits_{j=1}^{n} x_j \mathbf{G}_j > 0 \\ \mathbf{A}\mathbf{x} \geq \mathbf{b} \end{cases} \tag{3.2}$$

where $\mathbf{G}_j = \frac{\partial \boldsymbol{E}^*(\boldsymbol{r}_j)}{\partial \boldsymbol{\xi}^*} \cdot \frac{\partial \boldsymbol{E}(\boldsymbol{r}_j)}{\partial \boldsymbol{\xi}^{\mathrm{T}}} \in \mathbb{C}^{\nu\times\nu}$, $\mathbf{G}_j^{\mathrm{H}} = \mathbf{G}_j$, and

$$\mathbf{A} = \begin{pmatrix} \mathbf{I}_n \\ -\mathbf{1}^{\mathrm{T}} \end{pmatrix}, \qquad \mathbf{b} = \begin{pmatrix} \mathbf{0} \\ -1 \end{pmatrix} \tag{3.3}$$

where $\mathbf{I}_n$ is the $n \times n$ identity matrix, $\mathbf{1}$ an $n \times 1$ column vector of ones and $\mathbf{0}$ is an $n \times 1$ column vector of zeros. The matrix $\mathbf{A}$ is $m \times n$ and the vector $\mathbf{b}$ is $m \times 1$ where $m = n + 1$ with our present formulation (3.1).

The primal optimization problem (3.2) is now reformulated as

$$(\mathrm{P}) \begin{cases} \min\limits_{\mathbf{x},\mathbf{X}>0} -\log\det \mathbf{X} \\ \mathbf{X} - \mathbf{G}(\mathbf{x}) \geq 0 \\ -\mathbf{X} + \mathbf{G}(\mathbf{x}) \geq 0 \\ \mathbf{A}\mathbf{x} \geq \mathbf{b} \end{cases} \tag{3.4}$$

where $\mathbf{x} \in \mathbb{R}^n$ and the positive definite matrix variable $\mathbf{X} \in \mathbb{C}^{\nu\times\nu}$ has been introduced. Further, by introducing the positively semidefinite matrix Lagrange multipliers $\mathbf{W}_1 \in \mathbb{C}^{\nu\times\nu}$ and $\mathbf{W}_2 \in \mathbb{C}^{\nu\times\nu}$, and the non-negative vector Lagrange multiplier $\boldsymbol{\lambda} \in \mathbb{R}^m$, the problem (3.4) can be reformulated as

$$\min_{\mathbf{x},\mathbf{X}>0} \max_{\mathbf{W}_i\geq 0, \boldsymbol{\lambda}\geq\mathbf{0}} -\log\det \mathbf{X} - \mathrm{tr}\mathbf{W}_1(\mathbf{X} - \mathbf{G}(\mathbf{x})) - \mathrm{tr}\mathbf{W}_2(-\mathbf{X} + \mathbf{G}(\mathbf{x})) - \boldsymbol{\lambda}^{\mathrm{T}}(\mathbf{A}\mathbf{x} - \mathbf{b}). \tag{3.5}$$

Here, $(\mathbf{x}, \mathbf{X})$ are referred to as primal variables and $(\mathbf{W}_i, \boldsymbol{\lambda})$ as dual variables. It is readily seen that the optimal solution to (3.5) is characterized by

$$\mathbf{W}_1(\mathbf{X} - \mathbf{G}(\mathbf{x})) = \mathbf{0} \tag{3.6}$$

$$\mathbf{W}_2(-\mathbf{X} + \mathbf{G}(\mathbf{x})) = \mathbf{0} \tag{3.7}$$

$$\boldsymbol{\lambda}^{\mathrm{T}}(\mathbf{A}\mathbf{x} - \mathbf{b}) = 0. \tag{3.8}$$

The dual formulation is obtained by interchanging the order of minimization and maximization in (3.5)

$$\max_{\mathbf{W}_i\geq 0, \boldsymbol{\lambda}\geq\mathbf{0}} \min_{\mathbf{x},\mathbf{X}>0} -\log\det \mathbf{X} - \mathrm{tr}\mathbf{W}_1(\mathbf{X} - \mathbf{G}(\mathbf{x})) - \mathrm{tr}\mathbf{W}_2(-\mathbf{X} + \mathbf{G}(\mathbf{x})) - \boldsymbol{\lambda}^{\mathrm{T}}(\mathbf{A}\mathbf{x} - \mathbf{b}). \tag{3.9}$$

To perform the minimization in (3.9) the objective function $f(\mathbf{x}, \mathbf{X})$ is differentiated with respect to the primal variables

$$\frac{\partial f}{\partial x_j} = -\mathrm{tr}\left(\mathbf{W}_2 - \mathbf{W}_1\right)\mathbf{G}_j - \boldsymbol{\lambda}^{\mathrm{T}}\mathbf{a}_j = 0, \tag{3.10}$$

$$\frac{\partial f}{\partial \mathbf{X}} = -\mathbf{X}^{-1} + (\mathbf{W}_2 - \mathbf{W}_1) = \mathbf{0} \tag{3.11}$$

where $\mathbf{a}_j$ denote the columns of $\mathbf{A}$ and $j = 1, \ldots, n$. By employing (3.10) and (3.11) and introducing $\mathbf{W} = \mathbf{W}_2 - \mathbf{W}_1 = \mathbf{X}^{-1} > 0$, the function $f(\mathbf{x}, \mathbf{X})$ can now be written

$$f(\mathbf{x}, \mathbf{X}) = -\log\det\mathbf{X} + \mathrm{tr}\mathbf{W}\mathbf{X} - \mathrm{tr}\mathbf{W}\mathbf{G}(\mathbf{x}) - \boldsymbol{\lambda}^{\mathrm{T}}\left(\mathbf{A}\mathbf{x} - \mathbf{b}\right) = \log\det\mathbf{W} + \nu + \boldsymbol{\lambda}^{\mathrm{T}}\mathbf{b}. \tag{3.12}$$

Hence, the dual formulation (D) is

$$(\mathrm{D}) \begin{cases} \max\limits_{\mathbf{W}>0, \boldsymbol{\lambda}\geq\mathbf{0}} \log\det\mathbf{W} + \boldsymbol{\lambda}^{\mathrm{T}}\mathbf{b} + \nu \\ \mathrm{tr}\mathbf{W}\mathbf{G}_j + \mathbf{a}_j^{\mathrm{T}}\boldsymbol{\lambda} = 0, \;\; j = 1, \ldots, n. \end{cases} \tag{3.13}$$

A solution $\mathbf{x} \in \mathbb{R}^n$ is said to be primal feasible if the corresponding constraints of the primal problem (3.2) are satisfied. In particular, it is noted that a primal feasible solution $(\mathbf{x}, \mathbf{X})$ in (3.4) satisfies also $\mathbf{X} = \mathbf{G}(\mathbf{x})$. Accordingly, a solution $(\mathbf{W} > 0, \boldsymbol{\lambda} \geq \mathbf{0})$ is said to be dual feasible if the corresponding constraints of the dual problem (3.13) are satisfied. Since $\mathbf{W} = \mathbf{X}^{-1}$ as shown above, it is concluded that a primal and dual feasible solution $(\mathbf{x}, \mathbf{W}, \boldsymbol{\lambda})$ satisfies $\mathbf{W} = \mathbf{G}^{-1}(\mathbf{x})$ as well as $\boldsymbol{\lambda}^{\mathrm{T}}\left(\mathbf{A}\mathbf{x} - \mathbf{b}\right) \geq 0$.

The duality gap corresponding to a primal and dual feasible solution can now be calculated

$$\begin{aligned} DG &= -\log\det\mathbf{G}(\mathbf{x}) - \log\det\mathbf{W} - \boldsymbol{\lambda}^{\mathrm{T}}\mathbf{b} - \nu \\ &= \sum_{j=1}^{n} x_j\left(\mathrm{tr}\mathbf{W}\mathbf{G}_j + \boldsymbol{\lambda}^{\mathrm{T}}\mathbf{a}_j\right) - \boldsymbol{\lambda}^{\mathrm{T}}\mathbf{b} - \nu = \mathrm{tr}\mathbf{W}\mathbf{G}(\mathbf{x}) + \boldsymbol{\lambda}^{\mathrm{T}}\mathbf{A}\mathbf{x} - \boldsymbol{\lambda}^{\mathrm{T}}\mathbf{b} - \nu \\ &= \mathrm{tr}\mathbf{I}_\nu + \boldsymbol{\lambda}^{\mathrm{T}}\left(\mathbf{A}\mathbf{x} - \mathbf{b}\right) - \nu = \boldsymbol{\lambda}^{\mathrm{T}}\left(\mathbf{A}\mathbf{x} - \mathbf{b}\right) \geq 0. \end{aligned} \tag{3.14}$$

Hence, the duality gap is $DG = \boldsymbol{\lambda}^{\mathrm{T}}\left(\mathbf{A}\mathbf{x} - \mathbf{b}\right) \geq 0$ which is always non-negative. This means that the primal value is always greater than or equal to the dual value. From (3.8) we also see that an optimal solution is characterized by $DG = \boldsymbol{\lambda}^{\mathrm{T}}\left(\mathbf{A}\mathbf{x} - \mathbf{b}\right) = 0$ for which the primal and dual problems (3.2) and (3.13), respectively, have the same optimal value.

4 Solving the dual problem

Consider the dual problem formulation (3.13) in our particular application where $\mathbf{A}$ and $\mathbf{b}$ are given by (3.3). By partitioning the Lagrange multiplier vector $\boldsymbol{\lambda}$ as

$\boldsymbol{\lambda} = [\lambda_1, \ldots, \lambda_n,\ \mu]^{\mathrm{T}}$ the dual problem formulation (3.13) is now written

$$(D) \begin{cases} \max\limits_{\mathbf{W}>0, \lambda_j \geq 0, \mu \geq 0} \log\det \mathbf{W} - \mu + \nu \\ \mathrm{tr}\mathbf{W}\mathbf{G}_j + \lambda_j - \mu = 0,\ j = 1, \ldots, n. \end{cases} \tag{4.1}$$

By rewriting the equality constraints of (4.1) as inequality constraints using $\lambda_j \geq 0$, we obtain an equivalent convex optimization problem

$$(D) \begin{cases} \min\limits_{\mathbf{W}>0, \mu \geq 0} -\log\det \mathbf{W} + \mu - \nu \\ \lambda_j = -\mathrm{tr}\mathbf{W}\mathbf{G}_j + \mu \geq 0,\ j = 1, \ldots, n \end{cases} \tag{4.2}$$

where the decision variables have been reduced to $\mathbf{W} > 0$ and $\mu \geq 0$.

The advantage of solving (4.2) instead of (3.2) is that (4.2) comprises a small number of decision variables, assuming that $n \gg \nu^2$. If $\mathbf{W}$ is complex ($\boldsymbol{\xi}$ is complex), the corresponding number of real variables (including μ) is $\nu^2 + 1$. If $\mathbf{W}$ is real ($\boldsymbol{\xi}$ is real), the number of variables is $\frac{\nu(\nu+1)}{2} + 1$. Hence, we write

$$\mathbf{W} = \sum_{q=1}^{r} y_q \mathbf{W}_q \tag{4.3}$$

where y_q are real variables, the matrices $\mathbf{W}_q$ constitute a basis for $\mathbf{W}$ and r is either $r = \nu^2$ or $r = \frac{\nu(\nu+1)}{2}$ corresponding to the complex and real case, respectively. It is observed that the optimal solution of (4.2) can always be represented by a maximum of r active constraints. This follows from the Kuhn-Tucker conditions of (4.2) and an application of the Caratheodory's theorem as shown in the Appendix. Consequently, there are always a maximum of r optimal observation points $\boldsymbol{r}_j$ of (3.1) for which $x_j \geq 0$.

It has been previously established that an optimal measurement problem comprising of ν complex parameters can always be represented by a maximum of ν^2 optimal points (or $\frac{\nu(\nu+1)}{2}$ for the real case), see *e.g.*, [22]. By using the present duality theory, we see that the maximum number of optimal points r is equal to the number of dual parameters for the Fisher information matrix $\mathbf{G}$. Hence, if the Fisher information matrix has a specific structure such as the block diagonal structure in (2.4), then the dual variable $\mathbf{W}$ and its corresponding basis $\mathbf{W}_q$ attains the same structure. Thus, the corresponding number r of maximum observation points in this case may be much less then ν^2.

In order to solve (4.2) using an interior point algorithm [15, 24], we consider an unconstrained optimization problem using the following objective function

$$\varphi(\mathbf{y}, \mu, t) = t\left(-\log\det \mathbf{W} + \mu - \nu\right) - \sum_{j=1}^{n} \log \lambda_j - \log \mu \tag{4.4}$$

where $\mathbf{y}$ denotes an $r \times 1$ vector of y_q variables, the $\log\det(\cdot)$ and $\log(\cdot)$ functions are used as barriers for the feasible domains and t is a positive (large) number, cf. [7]. We note that (4.4) is a strictly convex function and we assume that it can

be minimized to any desired accuracy using e.g. very efficient Newton iterations. The resulting set of solution variables $(\mathbf{W}, \lambda_j, \mu)$ is strictly dual feasible for (4.2) assuming that such a solution exists, hence $\mathbf{W} > 0$, $\lambda_j > 0$ and $\mu > 0$. In fact, a strictly dual feasible initial solution for the Newton iterations is readily obtained by chosing $\mathbf{W} = \mathbf{I}$ and μ sufficiently large in (4.2).

The *central path* [7] is defined by the minimum of (4.4) and is characterized by

$$\begin{cases} \frac{\partial \varphi}{\partial y_q} = t\left(-\mathrm{tr}\mathbf{W}^{-1}\mathbf{W}_q\right) - \sum_{j=1}^{n} \frac{1}{\lambda_j}\left(-\mathrm{tr}\mathbf{W}_q\mathbf{G}_j\right) = 0 \\ \frac{\partial \varphi}{\partial \mu} = t - \sum_{j=1}^{n} \frac{1}{\lambda_j} - \frac{1}{\mu} = 0 \end{cases} \tag{4.5}$$

or, equivalently

$$\begin{cases} \mathrm{tr}\mathbf{W}^{-1}\mathbf{W}_q = \mathrm{tr}\sum_{j=1}^{n} \frac{1}{t\lambda_j}\mathbf{G}_j\mathbf{W}_q \\ \sum_{j=1}^{n} \frac{1}{t\lambda_j} + \frac{1}{t\mu} = 1. \end{cases} \tag{4.6}$$

Hence, from (4.6) we can chose

$$\begin{cases} x_j = \frac{1}{t\lambda_j} = \frac{1}{t\left(-\mathrm{tr}\mathbf{W}\mathbf{G}_j + \mu\right)} > 0 \\ \mathbf{G}(\mathbf{x}) = \sum_{j=1}^{n} x_j\mathbf{G}_j \end{cases} \tag{4.7}$$

and it is concluded that $\mathbf{W}^{-1} = \mathbf{G}(\mathbf{x}) > 0$, $\sum_{j=1}^{n} x_j < 1$, and $(\mathbf{x}, \mathbf{W}, \boldsymbol{\lambda})$ is a primal and dual feasible solution of (3.2). The corresponding duality gap is given by

$$DG = \boldsymbol{\lambda}^{\mathrm{T}}\left(\mathbf{A}\mathbf{x} - \mathbf{b}\right) = \sum_{j=1}^{n} \lambda_j x_j + \mu\left(-\sum_{j=1}^{n} x_j + 1\right) = \frac{n+1}{t}. \tag{4.8}$$

The duality theory makes it possible to determine a suitable value of t in order to solve (4.2) within a certain accuracy. Suppose *e.g.*, that we require a relative accuracy c (where $c = 0.99$ corresponds to 99% accuracy) so that the desired solution satisfies

$$c \det \mathbf{G}_o \leq \det \mathbf{G} \leq \det \mathbf{G}_o \tag{4.9}$$

where $\mathbf{G}_o$ denotes the optimal solution. It is then readily seen that the condition

$$DG \leq -\log c \tag{4.10}$$

implies that (4.9) is satisfied. Hence, a suitable value of t to use in (4.4) could be

$$t = \frac{2(n+1)}{-\log c} \tag{4.11}$$

so that the duality gap of the corresponding central path solution given by (4.8) is $DG = \frac{1}{2}(-\log c)$. The condition (4.10) can then be used as a stopping criteria for the Newton iterations. Thus, by employing a relative accuracy criterion for the $\max\det(\cdot)$ problem, an absolute accuracy criterion is obtained for the $\min\log\det(\cdot)$ problem for which the duality gap can be directly applied. A more sophisticated algorithm employs a combination of dual and primal central paths, as well as an iteration of the t-parameter, see *e.g.*, [7, 15, 24]. A staightforward interior point optimization algorithm to solve (4.2) is given in the Appendix.

5 Numerical examples

We consider a numerical example for the optimal measurement formulation (3.1), reformulated as a dual problem in (4.2) and by using the straightforward interior point optimization algorithm described in the Appendix. We employ as a measurement case the Fisher information matrix described in (2.4) and evaluate the resulting Cramér-Rao lower bound using (2.5).

We consider an antenna near-field estimation problem with fairly small electrical size, and assume that the number of excited modes is $L = 3$. We assume that the estimation is optimized for $ka = 2\pi$ at the radius of one wave length $a = \lambda$, and that the measurement is made at the cylindrical surface $\{\rho = 2\lambda, -5\lambda \leq z \leq 5\lambda\}$ with $n = 101$ positions z and $M = 120$ azimuthal points ϕ. As an illustration, we employ only a few parameters and consider an estimation problem for the three electrical TE modes ($\tau = 1, m = 1, l = 1, 2, 3$) as shown in Figure 2.

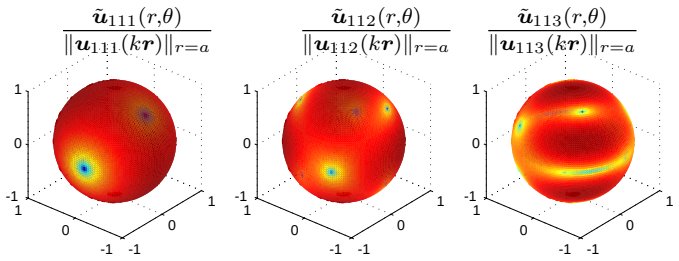

Figure 2: The three normalized electrical TE modes ($\tau = 1, m = 1, l = 1, 2, 3$) at radius $a = \lambda$.

In Figure 3 is shown the optimal solution x_j together with the magnitudes of the three electrical TE modes over the measurement domain. Hence, the optimization gives two optimal points at the position $z = \pm 0.7\lambda$. Note that these two vector measurements correspond to four scalar measurements which are thus optimal for estimating the three complex parameters $\{f_{11l}\}_{l=1,2,3}$. In Figure 4 is shown the optimization process over iteration index. The convergence of primal and dual costs is fairly slow using this straightforward interior point optization algorithm. However, the quantized solution, as described in the Appendix, shows a very fast convergence to the optimal solution.

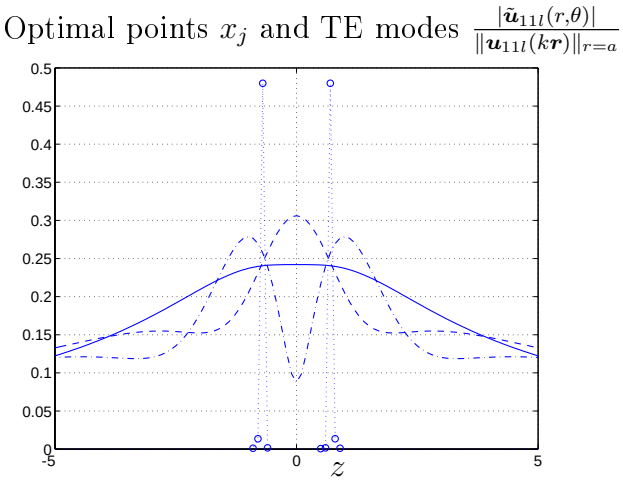

Figure 3: Optimal solution for the antenna near-field estimation of TE modes ($\tau = 1, m = 1, l = 1, 2, 3$) at radius $a = \lambda$. Dotted line with "o" indicate the optimal measurement points x_j. Solid, dashed and dash-dotted line show the TE modes for $l = 1, 2, 3$, respectively.

In Figure 5 a) and b) is shown the Cramér-Rao lower bound for near-field estimation (2.5) using the $z = \pm 5\lambda$ measurement, and the optimal measurement positions $z = \pm 0.7\lambda$, respectively. It is assumed here that the noise variance in (2.5) corresponds to a 50 dB signal to noise ratio at a signal level of 0 dB. Note that the estimation error in this example becomes somewhat more evenly spread using the $z = \pm 5\lambda$ measurement, whereas the overall estimation error is improved by 10-15 dB using the optimal measurement constellation.

6 Summary and conclusions

We introduce a mathematical framework for optimization of antenna near-field imaging problems, based on the multipole expansion of the electromagnetic field, the *Fisher information* to quantify the quality of data and use of modern interior point convex optimization techniques. The general problem of optimizing the measurement sensor allocation for parameter estimation in distributed systems is considered, as well as the specific problem of optimizing the measurement set-up for antenna near-field estimation based on cylindrical data. The convex optimization problem is examined using duality theory, and it is shown that several structural properties of the optimal measurement problem can be exploited in developing an efficient interior point optimization method. In particular, we show that the cylindrical measurement set-up yields a Fisher information matrix with block diagonal structure, a feature which can be directly exploited in the optimization algorithm by reducing the number of dual decision variables. The presented framework for optimization is particularly useful when the number of nonzero elements of the Fisher information matrix is much less then the number of possible measurement positions, a situation which is relevant for reasonable small antennas which can be characterized by a

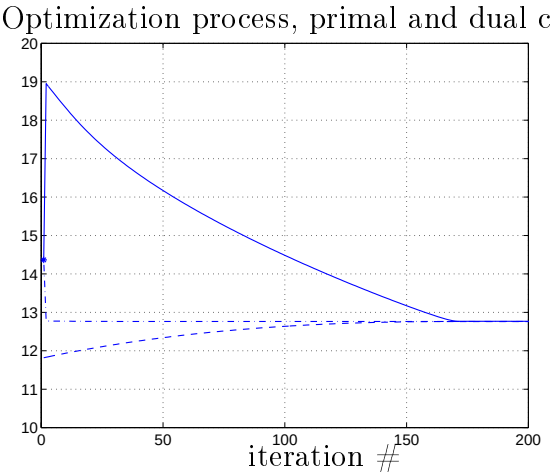

Figure 4: Optimization process. The solid, dashed and dash-dotted lines show the primal cost $-\log\det\mathbf{G}$, the dual cost $\log\det\mathbf{W}-\mu+\nu$ and the quantized primal cost, respectively.

limited number of vector modes.

Appendix A Spherical Vector Waves and their Azimuthal Fourier Transforms

The outgoing spherical vector waves are given by

$$\begin{aligned}\boldsymbol{u}_{1ml}(k\boldsymbol{r}) &= \mathrm{h}_l^{(2)}(kr)\boldsymbol{A}_{1ml}(\hat{\boldsymbol{r}})\\ \boldsymbol{u}_{2ml}(k\boldsymbol{r}) &= \frac{1}{k}\nabla\times\boldsymbol{u}_{1ml}(k\boldsymbol{r}) = \frac{(kr\mathrm{h}_l^{(2)}(kr))'}{kr}\boldsymbol{A}_{2ml}(\hat{\boldsymbol{r}}) + \sqrt{l(l+1)}\frac{\mathrm{h}_l^{(2)}(kr)}{kr}\boldsymbol{A}_{3ml}(\hat{\boldsymbol{r}})\end{aligned} \tag{A.1}$$

where $\boldsymbol{A}_{\tau ml}(\hat{\boldsymbol{r}})$ are the *spherical vector harmonics* and $\mathrm{h}_l^{(2)}(x)$ the *spherical Hankel functions of the second kind*, see [1, 6, 9]. The spherical vector harmonics $\boldsymbol{A}_{\tau ml}(\hat{\boldsymbol{r}})$ are given by

$$\begin{aligned}\boldsymbol{A}_{1ml}(\hat{\boldsymbol{r}}) &= \frac{1}{\sqrt{l(l+1)}}\nabla\times(\boldsymbol{r}\mathrm{Y}_{ml}(\hat{\boldsymbol{r}}))\\ \boldsymbol{A}_{2ml}(\hat{\boldsymbol{r}}) &= \hat{\boldsymbol{r}}\times\boldsymbol{A}_{1ml}(\hat{\boldsymbol{r}})\\ \boldsymbol{A}_{3ml}(\hat{\boldsymbol{r}}) &= \hat{\boldsymbol{r}}\mathrm{Y}_{ml}(\hat{\boldsymbol{r}})\end{aligned} \tag{A.2}$$

where $\mathrm{Y}_{ml}(\hat{\boldsymbol{r}})$ are the scalar *spherical harmonics* given by

$$\mathrm{Y}_{ml}(\theta,\phi) = (-1)^m\sqrt{\frac{2l+1}{4\pi}}\sqrt{\frac{(l-m)!}{(l+m)!}}\mathrm{P}_l^m(\cos\theta)\mathrm{e}^{\mathrm{i}m\phi} \tag{A.3}$$

and where $\mathrm{P}_l^m(x)$ are the *associated Legendre functions* [1]. For negative m-indices, the scalar waves satisfies the symmetry $\mathrm{Y}_{-m,l}(\hat{\boldsymbol{r}}) = (-1)^m\mathrm{Y}_{ml}^*(\hat{\boldsymbol{r}})$, and hence

$$\boldsymbol{A}_{\tau,-m,l}(\hat{\boldsymbol{r}}) = (-1)^m\boldsymbol{A}_{\tau ml}^*(\hat{\boldsymbol{r}}). \tag{A.4}$$

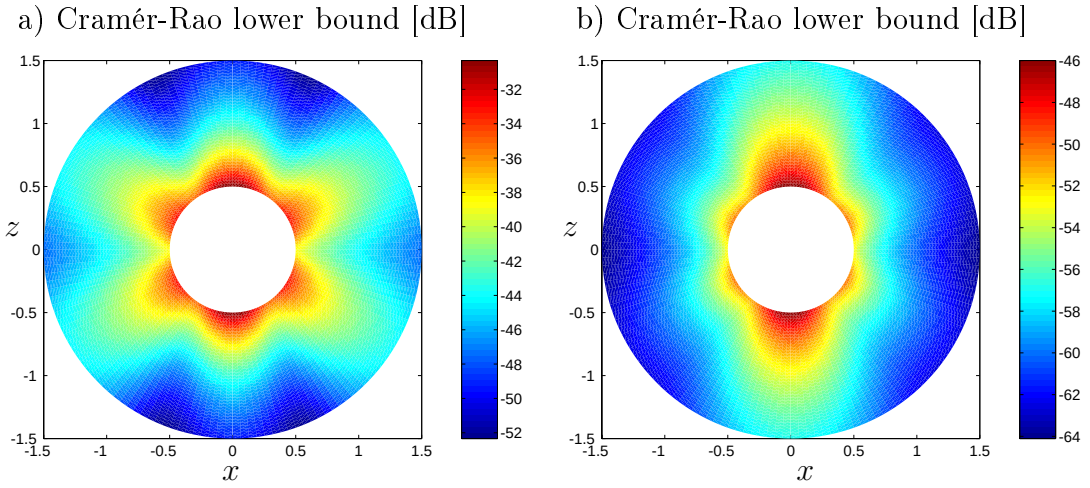

Figure 5: Cramér-Rao lower bound for near-field estimation plotted for $0.5\lambda \leq \rho \leq 1.5\lambda$, $0 \leq \theta \leq \pi$ and $\phi = 0, \pi$ (xz-plane). In a) using the measurement positions $z = \pm 5\lambda$ and in b) using the optimal measurement positions $z = \pm 0.7\lambda$.

For convenience, we introduce also the *normalized* associated Legendre functions

$$\bar{\mathrm{P}}_l^m(x) = \sqrt{\frac{2l+1}{2}}\sqrt{\frac{(l-m)!}{(l+m)!}}\mathrm{P}_l^m(x) \tag{A.5}$$

so that $\mathrm{Y}_{ml}(\hat{\boldsymbol{r}}) = (-1)^m \bar{\mathrm{P}}_l^m(\cos\theta)\frac{1}{\sqrt{2\pi}}\mathrm{e}^{\mathrm{i}m\phi}$. The following relations for $\bar{\mathrm{P}}_l^m(x)$ are useful for numerical calculations

$$\begin{aligned}
&\bar{\mathrm{P}}_l^{-m}(x) = (-1)^m \bar{\mathrm{P}}_l^m(x) \\
&\frac{\partial}{\partial\theta}\bar{\mathrm{P}}_l^m(x) = \frac{1}{2}\sqrt{(l+m)(l-m+1)}\bar{\mathrm{P}}_l^{m-1}(x) - \frac{1}{2}\sqrt{(l+m+1)(l-m)}\bar{\mathrm{P}}_l^{m+1}(x)
\end{aligned} \tag{A.6}$$

where $x = \cos\theta$. Note also that $\bar{\mathrm{P}}_l^m(x) = 0$ for $m > l$.

Now, from (A.2) the spherical vector harmonics may be derived as

$$\begin{aligned}
\boldsymbol{A}_{1ml}(\hat{\boldsymbol{r}}) &= \tilde{\boldsymbol{A}}_{1ml}(\theta)\mathrm{e}^{\mathrm{i}m\phi} = \frac{(-1)^m}{\sqrt{l(l+1)}}\left(\hat{\boldsymbol{\theta}}\frac{\mathrm{i}m}{\sin\theta}\bar{\mathrm{P}}_l^m(\cos\theta) - \hat{\boldsymbol{\phi}}\frac{\partial}{\partial\theta}\bar{\mathrm{P}}_l^m(\cos\theta)\right)\frac{1}{\sqrt{2\pi}}\mathrm{e}^{\mathrm{i}m\phi} \\
\boldsymbol{A}_{2ml}(\hat{\boldsymbol{r}}) &= \tilde{\boldsymbol{A}}_{2ml}(\theta)\mathrm{e}^{\mathrm{i}m\phi} = \frac{(-1)^m}{\sqrt{l(l+1)}}\left(\hat{\boldsymbol{\theta}}\frac{\partial}{\partial\theta}\bar{\mathrm{P}}_l^m(\cos\theta) + \hat{\boldsymbol{\phi}}\frac{\mathrm{i}m}{\sin\theta}\bar{\mathrm{P}}_l^m(\cos\theta)\right)\frac{1}{\sqrt{2\pi}}\mathrm{e}^{\mathrm{i}m\phi} \\
\boldsymbol{A}_{3ml}(\hat{\boldsymbol{r}}) &= \tilde{\boldsymbol{A}}_{3ml}(\theta)\mathrm{e}^{\mathrm{i}m\phi} = \hat{\boldsymbol{r}}(-1)^m\bar{\mathrm{P}}_l^m(\cos\theta)\frac{1}{\sqrt{2\pi}}\mathrm{e}^{\mathrm{i}m\phi}
\end{aligned} \tag{A.7}$$

where the *Fourier transformed* spherical vector harmonics $\tilde{\boldsymbol{A}}_{\tau ml}(\theta)$ are defined so that

$$\boldsymbol{A}_{\tau ml}(\hat{\boldsymbol{r}}) = \tilde{\boldsymbol{A}}_{\tau ml}(\theta)\mathrm{e}^{\mathrm{i}m\phi}. \tag{A.8}$$

The Fourier transformed outgoing spherical vector waves $\tilde{\boldsymbol{u}}_{\tau ml}(r,\theta)$ are derived similarly from (A.1) as

$$\begin{aligned}
\tilde{\boldsymbol{u}}_{1ml}(r,\theta) &= \mathrm{h}_l^{(2)}(kr)\tilde{\boldsymbol{A}}_{1ml}(\theta) \\
\tilde{\boldsymbol{u}}_{2ml}(r,\theta) &= \frac{(kr\mathrm{h}_l^{(2)}(kr))'}{kr}\tilde{\boldsymbol{A}}_{2ml}(\theta) + \sqrt{l(l+1)}\frac{\mathrm{h}_l^{(2)}(kr)}{kr}\tilde{\boldsymbol{A}}_{3ml}(\theta)
\end{aligned} \tag{A.9}$$

so that

$$\boldsymbol{u}_{\tau ml}(k\boldsymbol{r}) = \tilde{\boldsymbol{u}}_{\tau ml}(r,\theta)\mathrm{e}^{\mathrm{i}m\phi}. \tag{A.10}$$

Note that $\tilde{\boldsymbol{A}}_{\tau ml}(\theta)$ and $\tilde{\boldsymbol{u}}_{\tau ml}(r,\theta)$ are defined as Fourier transforms only with respect to their respective spherical r,θ,ϕ components. As vector fields they still depend on the ϕ coordinate via the basis vectors $\hat{\boldsymbol{r}},\hat{\boldsymbol{\theta}},\hat{\boldsymbol{\phi}}$.

Appendix B Maximum number of optimal points

We prove here that the optimal solution of (4.2) always can be represented by a maximum of r active constraints.

The Kuhn-Tucker conditions of (4.2) are given by

$$\begin{pmatrix} -\mathrm{tr}\mathbf{W}^{-1}\mathbf{W}_q \\ 1 \end{pmatrix} = \sum_{j=1}^{n} \zeta_j \begin{pmatrix} -\mathrm{tr}\mathbf{W}_q\mathbf{G}_j \\ 1 \end{pmatrix} \tag{B.1}$$

where ζ_j are non-negative Lagrange multipliers and $q = 1,\ldots,r$. Caratheodory's theorem [21] states that a vector $\mathbf{x} \in \mathbb{R}^r$ belongs to the convex cone$C$ generated by a set $G \subset \mathbb{R}^r$ if and only if $\mathbf{x}$ can be expressed as a non-negative linearcombination of r vectors in G. Hence, we may take $\mathbf{x} = (-\mathrm{tr}\mathbf{W}^{-1}\mathbf{W}_q) \in \mathbb{R}^r$ and $G = \{(-\mathrm{tr}\mathbf{W}_q\mathbf{G}_j)\}_{j=1}^n \subset \mathbb{R}^r$, and conclude that (B.1) can always be represented by a maximum of r multpliers $\zeta_j \geq 0$. It follows that there are always a maximum of r optimal observation points $\boldsymbol{r}_j$ of (3.1) for which $x_j \geq 0$.

Appendix C Interior point optimization algorithm

A straightforward interior point optimization algorithm to solve (4.2) is given below. As stopping criteria is used (4.10), and the parameter t is given by *e.g.*, (4.11).

1. Initialization. Initialize with $x_j = \frac{1}{n}$, and

$$\mathbf{G}(\mathbf{x}) = \frac{1}{n}\sum_{j=1}^{n}\mathbf{G}_j \tag{C.1}$$

$$\mathbf{W} = \mathbf{G}^{-1}(\mathbf{x}) \tag{C.2}$$

$$\mu = \max_{j\in\{1,\ldots,n\}} \mathrm{tr}\mathbf{W}\mathbf{G}_j + \varepsilon \tag{C.3}$$

$$\lambda_j = -\mathrm{tr}\mathbf{W}\mathbf{G}_j + \mu,\ j = 1,\ldots,n \tag{C.4}$$

where $\varepsilon > 0$ is a small positive number. This initialization is stricytly dual feasible, hence $\mathbf{W} > 0$, $\lambda_j > 0$ and $\mu > 0$.

2. Newton iteration. Make K Newton iterations on the unconstrained function $\varphi(\mathbf{y},\mu,t)$ in (4.4). Denote the kth variable vector

$$\mathbf{u}_k = \begin{pmatrix} \mathbf{y}_k \\ \mu_k \end{pmatrix} \tag{C.5}$$

and calculate the corresponding gradient $\mathbf{g}_k$ from

$$\begin{cases} \frac{\partial\varphi}{\partial y_q} = -t\mathrm{tr}\mathbf{W}^{-1}\mathbf{W}_q + \sum_{j=1}^{n}\frac{1}{\lambda_j}\mathrm{tr}\mathbf{W}_q\mathbf{G}_j \\ \frac{\partial\varphi}{\partial\mu} = t - \sum_{j=1}^{n}\frac{1}{\lambda_j} - \frac{1}{\mu} \end{cases} \tag{C.6}$$

and Hessian $\mathbf{H}_k$ from

$$\begin{cases} \frac{\partial^2\varphi}{\partial y_p\partial y_q} = t\mathrm{tr}\mathbf{W}^{-1}\mathbf{W}_p\mathbf{W}^{-1}\mathbf{W}_q + \sum_{j=1}^{n}\frac{1}{\lambda_j^2}\mathrm{tr}\mathbf{W}_p\mathbf{G}_j\mathrm{tr}\mathbf{W}_q\mathbf{G}_j \\ \frac{\partial^2\varphi}{\partial y_q\partial\mu} = -\sum_{j=1}^{n}\frac{1}{\lambda_j^2}\mathrm{tr}\mathbf{W}_q\mathbf{G}_j \\ \frac{\partial^2\varphi}{\partial\mu^2} = \sum_{j=1}^{n}\frac{1}{\lambda_j^2} + \frac{1}{\mu^2} \end{cases} \tag{C.7}$$

where $p, q = 1, \ldots, r$.

The Newton iteration is now given by

$$\mathbf{p}_k = -\mathbf{H}_k^{-1}\mathbf{g}_k \tag{C.8}$$

$$\|\mathbf{p}_k\|_H = \sqrt{\mathbf{p}_k^{\mathrm{T}}\mathbf{H}_k\mathbf{p}_k} \tag{C.9}$$

$$\mathbf{u}_{k+1} = \mathbf{u}_k + d_k\mathbf{p}_k \tag{C.10}$$

where $\mathbf{p}_k$ and $\|\mathbf{p}_k\|_H$ are referred to as the *Newton direction* and the *Newton decrement*, respectively, and where the step-length parameter d_k can be chosen as e.g.

$$d_k = \begin{cases} 1 & \text{if } \|\mathbf{p}_k\|_H \le \frac{1}{2} \\ \frac{1}{1+\|\mathbf{p}_k\|_H} & \text{if } \|\mathbf{p}_k\|_H > \frac{1}{2}. \end{cases} \tag{C.11}$$

It can be shown that the choice of step-length parameter as in (C.11) will guarantee that the iterations result in strictly dual feasible variables ($\mathbf{W} > 0, \lambda_j = -\mathrm{tr}\mathbf{W}\mathbf{G}_j + \mu > 0, \mu > 0$), see e.g. [7, 15]. The dual cost is now given by $\log\det\mathbf{W} - \mu + \nu$ as in (4.1) and the primal cost $-\log\det\mathbf{G}$ in (3.2) can be obtained by calculating the primal variables as in (4.7).

3. Truncation of primal variables. Chose the r largest values of $x_j = \frac{1}{t\lambda_j}$ and set the rest of the $\xi_j = 0$. Scale the variables so that $\sum_{x_j\neq 0} x_j = 1$. Calculate $\mathbf{G}(\mathbf{x}) = \sum_{x_j\neq 0} x_j\mathbf{G}_j$ and the corresponding primal cost $-\log\det\mathbf{G}(\mathbf{x})$. If $\mathbf{G}(\mathbf{x})$ is singular, or nearly singular, return to step 2 above.

4. Accuracy calculation. Calculate the dual variables

$$\mathbf{W} = \mathbf{G}^{-1}(\mathbf{x}) > 0 \tag{C.12}$$

$$\mu = \max_{j\in\{1\ldots n\}} \mathrm{tr}\mathbf{W}\mathbf{G}_j \ge 0 \tag{C.13}$$

$$\lambda_j = -\mathrm{tr}\mathbf{W}\mathbf{G}_j + \mu \ge 0,\ j = 1, \ldots, n. \tag{C.14}$$

The corresponding primal and dual variables are now primal and dual feasible, and we may calculate the duality gap

$$DG = \sum_{j=1}^{n} \lambda_j x_j + \mu \left(-\sum_{j=1}^{n} x_j + 1 \right) = \sum_{x_j \neq 0} \lambda_j x_j. \tag{C.15}$$

If $DG \leq -\log c$, then stop according to the stopping criteria as described above, see (4.10). Else, return to step 2 above, and use the previous set of dual variables $(\mathbf{W}, \lambda_j, \mu)$ from step 2 as initialization. □

Appendix Acknowledgement

The authors gratefully acknowledge the financial support by the Swedish Research Council.

References

[1] G. B. Arfken and H. J. Weber. *Mathematical Methods for Physicists.* Academic Press, New York, fifth edition, 2001.

[2] A. C. Atkinson and A. N. Donev. *Optimum Experimental Designs.* Oxford Statistical Science Series. Oxford University Press, Oxford, 1992.

[3] I. Bauer, H. G. Bock, S. Körkel, and J. P. Schlöder. Numerical methods for optimum experimental design in DAE systems. *Journal of Computational and Applied Mathematics*, **120**(1–2), 1–25, 2000.

[4] M. Bertero. Linear inverse and ill–posed problems. *Advances in electronics and electron physics*, **75**, 1–120, 1989.

[5] M. Gustafsson. *Wave Splitting in Direct and Inverse Scattering Problems.* PhD thesis, Lund Institute of Technology, Department of Electromagnetic Theory, P.O. Box 118, S-221 00 Lund, Sweden, 2000. `http://www.es.lth.se/home/mats`.

[6] J. E. Hansen, editor. *Spherical Near-Field Antenna Measurements.* Number 26 in IEE electromagnetic waves series. Peter Peregrinus Ltd., Stevenage, UK, 1988. ISBN: 0-86341-110-X.

[7] D. Hertog. *Interior Point Approach to Linear, Quadratic and Convex Programming.* Kluwer Academic Publishers, 1994.

[8] V. Isakov. *Inverse Problems for Partial Differential Equations.* Springer-Verlag, Berlin, 1998.

[9] J. D. Jackson. *Classical Electrodynamics.* John Wiley & Sons, New York, second edition, 1975.

[10] S. M. Kay. *Fundamentals of Statistical Signal Processing, Estimation Theory.* Prentice-Hall, Inc., NJ, 1993.

[11] A. Kirsch. *An Introduction to the Mathematical Theory of Inverse Problems.* Springer-Verlag, New York, 1996.

[12] E. A. Marengo and A. J. Devaney. The inverse source problem of electromagnetics: Linear inversion formulation and minimum energy solution. *IEEE Trans. Antennas Propagat.*, **47**(2), 410–412, February 1999.

[13] E. A. Marengo, A. J. Devaney, and F. K. Gruber. Inverse source problem with reactive power constraint. *IEEE Trans. Antennas Propagat.*, **52**(6), 1586–1595, June 2004.

[14] E. A. Marengo and R. W. Ziolkowski. Nonradiating and minimum energy sources and their fields: Generalized source inversion theory and applications. *IEEE Trans. Antennas Propagat.*, **48**(10), 1553–1562, October 2000.

[15] Y. Nesterov and A. Nemirovsky. *Interior Point Polynomial Methods in Convex Programming*, volume 13. Studies in Applied Mathematics, Society for Industrial and Applied Mathematics, Philadelphia, PA, 1994.

[16] S. Nordebo, M. Gustafsson, and K. Persson. Sensitivity analysis for antenna near-field imaging. Technical Report LUTEDX/(TEAT-7139)/1–17/(2005), Lund Institute of Technology, Department of Electroscience, P.O. Box 118, S-211 00 Lund, Sweden, 2005. `www.es.lth.se/teorel/`.

[17] S. Nordebo and M. Gustafsson. Multichannel broadband Fano theory for arbitrary lossless antennas with applications in DOA estimation. In *2005 IEEE International Conference on Acoustics, Speech, and Signal Processing*, volume IV, pages 969–972, 2005.

[18] S. Nordebo and M. Gustafsson. Statistical signal analysis for the inverse source problem of electromagnetics. Technical Report LUTEDX/(TEAT-7136)/1–12/(2005), Lund Institute of Technology, Department of Electroscience, P.O. Box 118, S-211 00 Lund, Sweden, 2005. `http://www.es.lth.se/teorel`, Accepted by IEEE Trans. Signal Process.

[19] F. Pukelsheim. *Optimal Design of Experiments.* Wiley Series in Probability and Mathematical Statistics. Wiley, New York, 1993.

[20] Z. H. Qureshi, T. S. Ng, and G. C. Goodwin. Optimum experimental design for identification of distributed parameter systems. *International Journal on Control*, **31**, 21–29, 1980.

[21] R. T. Rockafellar. *Convex Analysis.* Princeton University Press, Princeton, N. J., 1969.

[22] D. Ucinski and J. Korbicz. Optimal sensor allocation for parameter estimation in distributed systems. *Journal of Inverse and Ill–Posed Problems*, **9**(3), 301–317, 2001.

[23] M. van de Wal and B. de Jager. A review of methods for input/output selection. *Automatica*, **37**(4), 487–510, 2001.

[24] L. Vandenberghe, S. Boyd, and S.-P. Wu. Determinant maximization with linear matrix inequality constraints. *SIAM Journal on Matrix Analysis & Applications*, **19**(2), 499–534, 1998.

[25] A. V. Wouwer, N. Point, S. Porteman, and M. Remy. An approach to the selection of optimal sensor locations in distributed parameter systems. *Journal of Process Control*, **10**(4), 291–300, 2000.